SPE 84374

Modeling of Performance Behavior in Gas Condensate Reservoirs Using a Variable Mobility Concept

B.W. Wilson, Baker Atlas, R.A. Archer, University of Auckland, and T.A. Blasingame, Texas A&M U.

This paper was prepared for presentation at the SPE Annual Technical Conference and Exhibition held in Denver, CO., 5-8 October 2003.

Abstract

This work provides a concept for modelling well performance behavior in a gas condensate reservoir using an empirical model for the gas mobility function. This model is given by:

$$k = k_{min} + (k_{max} - k_{min}) \left[1 - \exp\left[\frac{-1}{\alpha} \frac{r^2}{t} \right] \right]$$

This concept model represents the minimum gas permeability (or mobility) near the wellbore and the maximum (or original) gas permeability (or mobility) in the "dry gas" portion of the reservoir, as well as the transition regime. This model was constructed based on observations derived from numerical simulation results where the saturation, effective permeability, and gas mobility are presented as functions of distance in the reservoir.

The utility of this concept is that it can be used to develop a pressure solution for the behavior of the gas phase produced from a gas condensate reservoir. This new solution is validated against numerical simulation and has been presented graphically for use in well test analysis (in the form of "type curves"). The advantage of this solution over the conventional radial composite reservoir solutions is that the evolution of the condensate zone can be represented and evaluated as it occurs in time. The obvious limitation is the simplified form of the k_g profile as a function of radius and time, as well as the dependence/appropriateness of the "α" coefficient.

Application of this new pressure solution to well test analysis is proposed — and comparisons to the radial composite (and other reservoir models) are also presented. Our goal is to demonstrate that the proposed solution has potential utility in the analysis and interpretation of reservoir performance data (most likely, pressure drawdown and pressure buildup test data).

We recognize that the simplicity of this approach may have practical limitations — for example, we consider a radially-varying mobility profile, but we also assume a constant diffusivity — this is a potential shortcoming that should be considered in future work.

Objectives

The primary objective of this work is:

- To develop an analytical representation of the pressure behavior in time and space for a reservoir system with a varying mobility profile (see **Fig. 1** for the mobility profile observed from numerical simulation for a radial gas condensate reservoir system).

The secondary objectives of this work are:

- To utilize this new model as a mechanism to develop graphical solutions for the pressure derivative in time and radial distance so that the new solution can be compared to other solutions (*e.g.*, the 2-zone radial composite reservoir model and various cases of the sealing fault model (time derivative) — as well as the pressure and pressure derivative (radial derivative) as a function of radial distance derived from numerical simulation).
- To use this new model to develop solutions which include wellbore storage and skin effects for modeling the pressure drop and pressure drop derivative functions in time.
- To propose applications in the analysis of well test data acquired from pressure drawdown or pressure buildup tests.

Statement of Problem

This work is focused on the concept of using a functional form to represent a prescribed mobility profile (*i.e.*, k/μ) and to incorporate this empirically-derived model into the rigorous diffusivity equation for the liquid case. The goal is to use this concept and the resulting flow model to represent the gas condensate case. We are treating this case as a "liquid equivalent" problem where non-idealities (*e.g.*, pressure-dependent PVT functions) are addressed using the conventional pseudofunctions (*i.e.*, pseudopressure and pseudotime).

We have used the simulation cases presented by Roussennac[1] as a starting point for establishing a model for gas mobility as a function of radius and time for a gas condensate reservoir. We recognize that simulated profiles are problematic (*i.e.*, a different set of input data may yield a different profile), but we believe that the cases presented by Roussenac offer an appro-

priate starting point as these cases are well calibrated and veri-fied.

Using the results presented by Roussenac (see **Fig. 1**); we have established the following *conceptual* model for representing the permeability as a function of radius and pressure:

$$k = k_{min} + (k_{max} - k_{min})\left[1 - \exp\left[\frac{-1}{\alpha}\frac{r^2}{t}\right]\right] \quad \text{..... (1)}$$

The appropriate form of the diffusivity equation for this work is given as:

$$\frac{1}{r}\frac{\partial}{\partial r}\left[kr\frac{\partial p}{\partial r}\right] = \frac{1}{0.0002637}\phi\mu c_t\frac{\partial p}{\partial t} \text{ (Field units)} \quad \text{..... (2)}$$

Recall that we have presumed a "liquid equivalent" case (*i.e.*, there are no pressure dependent properties). As such, Eq. 1 is used as the permeability model and is coupled with the radial flow diffusivity equation for this case (Eq. 2) then solved for the case of a well produced at a constant rate in an infinite-acting reservoir. The relevant forms of this solution are derived in Appendix A and presented below.

"Pressure Solution"

$$p_D = \frac{1}{2}[k_{min}/k_{max}]^{\frac{\alpha_D}{4}} \times \int_{\varepsilon_D}^{\infty}\left[\frac{1}{\varepsilon_D}\exp\left[-\frac{\left[1+\frac{4}{\alpha_D}\right]}{\frac{4}{\alpha_D}}\ln[e^{-\frac{4}{\alpha_D}\varepsilon_D} - (1-k_{min}/k_{max})] + \frac{4}{\alpha_D}\varepsilon_D\right]\right]d\varepsilon_D \quad \text{..... (3)}$$

"Pressure Derivative in Time"

$$t_D\frac{\partial p_D}{\partial t_D} = \frac{1}{2}[k_{min}/k_{max}]^{\frac{\alpha_D}{4}} \times \exp\left[-\frac{\left[1+\frac{4}{\alpha_D}\right]}{\frac{4}{\alpha_D}}\ln[e^{-\frac{4}{\alpha_D}\frac{r_D^2}{4t_D}} - (1-k_{min}/k_{max})] + \frac{4}{\alpha_D}\frac{r_D^2}{4t_D}\right] \quad \text{..... (4)}$$

"Pressure Derivative in Radial Distance"

$$-r_D\frac{\partial p_D}{\partial r_D} = [k_{min}/k_{max}]^{\frac{\alpha_D}{4}} \times \exp\left[-\frac{\left[1+\frac{4}{\alpha_D}\right]}{\frac{4}{\alpha_D}}\ln[e^{-\frac{4}{\alpha_D}\frac{r_D^2}{4t_D}} - (1-k_{min}/k_{max})] + \frac{4}{\alpha_D}\frac{r_D^2}{4t_D}\right] \quad \text{..... (5)}$$

The most important issue to consider in evaluating Eqs. 3-5 is that no limiting assumptions are made (other than the traditional solution approach using the Boltzmann transform) and each formulation is presumed to be unique. We will note that Eq. 3 cannot be expressed analytically and must be evaluated numerically. In our case we have utilized the software *Mathematica*,[2] which is computationally flexible, as well as capable of generating "near exact" results. Eqs. 4 and 5 are closed form results that are essentially identical in form, we note that comparison of Eqs. 4 and 5 yield the following iden-tity:

$$2t_D\frac{\partial p_D}{\partial t_D} = -r_D\frac{\partial p_D}{\partial r_D} \quad \text{..... (6)}$$

Where (as noted in Appendix A), Eq. 6 is uniquely valid for this case as well as the homogeneous reservoir solution.

For plotting the pressure derivative functions in both time and space we have defined the following definitions: (which are derived by inspection of Eqs. 4 and 5)

$$p_{Ddt} = t_D\frac{\partial p_D}{\partial t_D} \quad \text{..... (7)}$$

$$p_{Ddr} = \left|r_D\frac{\partial p_D}{\partial r_D}\right| \quad \text{..... (8)}$$

Presentation of Results — Pressure Solution for the Case of a Permeability Profile that Varies with Time and Radial Distance

The new solution is presented in the following formats:

- p_{Ddt} versus $\alpha_D t_D/r_D^2$: (**Fig. 2**) This format provides perspective on "early" and "late" behavior, where for a particular value of α_D we can observe the evolution of the permeability profile in the pressure derivative response. The generalized *x*-axis plotting function permits us to view all possible scenarios of the α_D - parameter on the same plot.
- $p_D(\varepsilon_D)$ versus $r_D^2/(\alpha_D t_D)$: (**Fig. 3a**) This format illustrates the radial distribution of dimensionless pressure (analogous to pressure drop). We immediately note that the highest values of pressure drop (or dimensionless pressure, p_D) occur near the well (*i.e.*, at small r_D values)). For comparison, we note that, near the well, the lowest values of p_D occur for the homogeneous reservoir case (*i.e.*, k_{min}/k_{max}=0) — this confirms our concept that the evolving permeability profile acts to reduce flow near the well.
- p_{Ddr} versus $r_D^2/(\alpha_D t_D)$: (**Fig. 3b**) We note that, in the formats used in these plots, **Figs. 2 and 3b** are essentially "mirror images" — which is the behavior we expect when we consider the identity given by Eq. 9. **Fig. 3b** (as **Fig. 3a**) has little practical application (we do not measure pressures in the reservoir) — however, we will use both **Figs. 3a and 3b** to evaluate/validate a numerical simulation where pressure is provided as a function of radius.

Validation

Pressure Behavior in Radial Distance

A cursory validation of the new solution is achieved by comparison of the solution (specifically, the p_D and p_{Ddr} formulations) with results obtained from the literature (Roussenac (ref. 1)). In **Fig. 4a** we present the p_D—Δp (*i.e.*, $\Delta p = p_i - p_r$) match for this case and the p_{Ddr}—$|r(dp/dr)|$ match is shown in **Fig. 4b**. With the exception of the behavior near the well (*i.e.*, for small *r*-values), we note an excellent match of the data with the proposed solution.

The behavior at small values of *r* is dominated by the "skin zone" — actually a region of specified permeability used to provide the effect of near-well damage. We do not consider

the existence of a "near-well damage" zone, we simply model a propagating permeability profile as shown in **Fig. 1**. In **Fig. 5** we present the Δp and $|r(dp/dr)|$ data along with the Δp and $|r(dp/dr)|$ functions computed using our new reservoir model. Using **Fig. 5** we have attempted to identify/classify the flow regimes which were observed during this simulation. We note that this comparison of data and our proposed solution provides a strong validation of the proposed solution.

Pressure Behavior in Time

Our goal is to provide a qualitative comparison of the new proposed solution (time format result) and the 2-zone radial composite reservoir model — where we note that the radial composite model is the most commonly used reservoir model for the interpretation and analysis of well test data from gas condensate reservoirs.

We also present a comparison of the proposed model with the model for a well in the vicinity of one or more "sealing faults" — where our goal is to simply compare the influence of our new model as a "flow constricttion" or "flow barrier." We are not advocating the use of the "sealing faults" models for the analysis and interpretation of well performance data in gas condensate reservoir systems; we are simply making a qualitative (graphical) comparison of the solutions.

In **Fig. 6** we present the solution for a well in the vicinity of one or more sealing faults — this presentation clearly indicates that the orientation and number of faults dramatically affects the behavior of the p_{Ddt} function. In **Fig. 7** we present the "unified" plot (p_{Ddt} function) for multiple cases of the radial composite reservoir solution. The most important, and most relevant issue is that the radial composite solution has fixed mobility and diffusivity ratios (for the inner and outer zones) — by contrast to our solution which uses a permeability profile in radius and time, *but only a single value of diffusivity for the entire reservoir*. As such, we will only compare cases for the radial composite reservoir model where the diffusivity ratio is unity.

In **Fig. 8** we present a combined plot of all three reservoir cases: the sealing faults case, the 2-zone radial composite reservoir case, and our proposed reservoir model for a permeability profile which varies in time and radial distance. We note surprising similarity in the results shown in **Fig. 8** — despite the fact that the reservoir models shown have little in common. One interpretation could be that this behavior is a cause for concern since the models are distinctly different, yet produce similar behavior. Another interpretation could be that the 2-zone (fixed) radial composite reservoir model and the new propagating permeability profile model have, at least in concept, a common denominator of 2 dominant permeabilities (*i.e.*, the "near well" and "reservoir" permeabilities).

In fact, as we note from **Fig. 8**, the radial composite and propagating permeability solutions converge at "late times," — *i.e.*, when the reservoir permeability dominates the pressure response. This is an important validation as the models do agree uniquely at late times. We conclude that this comparison suggests utility of our new model for the analysis of well test data in gas condensate reservoirs — with the caveat that we noted earlier regarding the fact that our proposed model uses a single value of diffusivity, and the 2-zone composite reservoir model uses 2 distinct diffusivities (*i.e.*, the "near well" and the "reservoir" diffusivities).

The issue of the "sealing faults" model is somewhat more complex — we will simply suggest that a "flow barrier" (*i.e.*, a sealing fault) and a flow contrast (*i.e.*, the 2-zone radial composite reservoir model and the propagating permeability model) have similar (though not identical) behavior because the flow barrier/contrast affects the pressure behavior in a similar fashion. This conclusion is somewhat inductive, but we believe it is both plausible and relevant.

Addition of Wellbore Storage Effects

In our work so far we have only considered the case of an ideal well in an infinite-acting reservoir with a propagating permeability profile — where the well is produced at a constant rate. In this section we provide a mechanism for adding wellbore storage effects to our new solution for a propagating permeability profile. Wellbore storage is typically "added" to the base pressure solution using convolution (or superposition) — where convolution should be valid for this problem because we have assumed that are no non-linearities in the governing differential equation (Eq. 2). As such, the convolution for wellbore storage is written as:

$$p_{wD} = \int_0^{t_D} \frac{d}{d\tau}\left[q_{Dwbs}(\tau)\right] p_{sD}(t_D - \tau)\, dt_D \quad \text{..... (9)}$$

Where the q_D function (dimensionless sandface rate profile) is given as follows for the wellbore storage model:

$$q_{Dwbs} = \frac{q_{sf}}{q_{sur}} = 1 - C_D \frac{d}{dt_D}\left[p_{wD}\right] \quad \text{..... (10)}$$

And:

$$p_{sD} = p_D + s \quad \text{..... (11)}$$

Eqs. 9 and 10 can be combined to yield a "recursion relation" for the wellbore storage dimensionless pressure, p_{wD}, but this approach is tedious and prone to error propagation. Typical implementations of Eqs. 9 and 10 involve the use of the Laplace transformation — unfortunately, our proposed solution (Eq. 3) is not suited to the use of the Laplace transform, and, as such, we must resort to another approach.

For convenience we employ the method by Blasingame, *et al.*[3] for generating pressure solutions which include wellbore storage and skin effects — the solution used in this work is given in Appendix B.

We provide **Figs. 9a and 9b** as validations for the Blasingame, *et al.* method — specifically for the case of an infinite-acting homogeneous reservoir. The p_{wDt} function is computed using the procedures given in Appendix B and the p_{wDdt} function is computed using the procedures given in Appendix C (where we note that we have used a polynomial regression (a 3-point formula) to calculate the p_{wDdt} function. We note excellent agreement between the "exact" solutions (*i.e.*, the numerical inversion solution) and the approximate solutions provided by the methods given in ref. 3. By extension, we will apply the procedures given in Appendices B and C to our new solution for a radially propagating permeability function.

In **Figs. 10a-10f** we provide a sequence of solutions for the specific case of C_D=1x10^3 and k_{min}/k_{max} varying for each case

from $1x10^{0}$ to $1x10^{-3}$. Individual plots consider a single value of α_D, and the following cases of α_D=$1x10^{0}$, 10^{-1}, 10^{-2}, 10^{-3}, 10^{-4}, 10^{-5} are considered (**Figs. 10a-10f**, respectively). In **Figs. 10a-10f** we note the "evolving" effects of the α_D-parameter, and we comment that non-unique effects are possible (*i.e.*, a particular case or trend which appears similar to another case, although these cases have substantially different base properties (*e.g.*, k_{min}/k_{max}, α_D, etc.)). Most of the cases in **Figs. 10a-10f** should be described as unique (although **Figs. 10b and 10c** do appear to be very similar).

Our objective in this section is two-fold – first we wanted to present the development of wellbore storage solutions using our new radially propagating permeability result. Second, we want to establish the general character/behavior of such results. In **Fig. 11** we present a "composite" plot of all p_{wDdt} trends generated for C_D=$1x10^{3}$. We note distinct behavior for each case and we suggest that the character in these wellbore storage solutions (for this particular case) is both accurate and distinct. Similarly, in **Fig. 12** we present the same suite of solutions for C_D=$1x10^{20}$. The most obvious comment that we can make is that virtually all of the trends generated for the C_D=$1x10^{20}$ case are dominated by wellbore storage effects — *i.e.*, the α_D-parameter has virtually no influence on the response of the solution for the C_D=$1x10^{20}$ case.

The Pressure Buildup Case

In this work we presume that the proposed solution is "linear" in that there are no pressure-dependent coefficients in the governing differential equation. As linearity is presumed, we can use the theorem of superposition to account for the variation of rate which occurs in a pressure buildup test (we make the conventional assumption that a "pressure buildup" is a period of zero rate, preceded by a period of production, t_p, at a constant flowrate.

The mathematical expression of superposition for this case is given in the form of dimensionless pressure and time as fol-lows:[4]

$$p_{wD,BU} = \frac{1}{141.2}\frac{k_{max}h}{qB\mu}\left(p_{ws}(\Delta t) - p_{wf}(\Delta t = 0)\right)$$
$$= p_{wD}(\Delta t_{pD}) - p_{wD}(t_{pD} + \Delta t_D) + p_{wD}(\Delta t_D) \quad \ldots\ldots (9)$$

We have used Eq. 7 to generate a series of cases where the α_D and C_D parameters are held constant (α_D=$1x10^{-3}$, and C_D=$1x10^{3}$), where and t_{pD} and k_{min}/k_{max} are varied. The variance in the k_{min}/k_{max} parameter provides a "span" of outcomes which illustrate the influence of the variable mobility function. In addition, only a single value of the α_D and C_D parameters is used in order to capture the specific influence of the t_{pD} and k_{min}/k_{max} parameters.

Figs. 13a-13d illustrate cases for t_{pD}=$1x10^{3}$, 10^{6}, 10^{9}, 10^{12} — respectively, where both the p_{wD} and p_{wDdt} functions are plotted versus $\Delta t_D/C_D$. For the t_{pD}=$1x10^{3}$ case (**Fig. 13a**) we note an extreme influence of the producing time (t_{pD}). In **Fig. 13b** (t_{pD}=$1x10^{6}$) we note that producing time (t_{pD}) does have a strong influence, but at least part of the response is unaffected by t_{pD} effects at early times (small $\Delta t_D/C_D$ values). For the case of t_{pD}=$1x10^{9}$ (**Fig. 13c**) we find that t_{pD} effects are only evident at late times (large $\Delta t_D/C_D$ values) — this is expected since $(\Delta t_D/C_D)_{max}C_D$=$\Delta t_{D,max}$=$1x10^{9}$. As such, $\Delta t_{D,max}/t_{pD}$=1, and we would expect some influence of producing time effects (by analogy with the homogeneous reservoir solution). Our final comparison, **Fig. 13d**, for the case of t_{pD}=$1x10^{12}$ we find no evidence of producing time effects — which is expected since $(\Delta t_D/C_D)_{max}C_D$=$\Delta t_{D,max}$=$1x10^{9}$ and $\Delta t_{D,max}/t_{pD}$=0.1 (the "drawdown" period is ten times the duration of the "buildup" period).

In **Fig. 14** we present a comparison of the time derivative functions (p_{wDdt}) versus $\Delta t_D/C_D$ for all of the pressure buildup solutions as well as the pressure drawdown solution. This comparison is useful to gauge the influence of t_{pD} relative to the base solution (*i.e.*, the drawdown solution). We can assess the qualitative influence of t_{pD} as being none (t_{pD}=$1x10^{12}$), to moderate (t_{pD}=$1x10^{9}$), to significant (t_{pD}=$1x10^{6}$), to extreme (t_{pD}=$1x10^{3}$).

We also considered cases where no wellbore storage effects in-fluence the pressure buildup solution — and we would note that similar comments regarding the influence of the t_{pD}-parameter can be made. We elected to focus on cases which do include wellbore storage (and skin) effects in order to assess the practical influence of the t_{pD}-parameter. We will note that, as with the homogeneous reservoir case, producing time effects can be addressed (at least approximately) using the "effective time" correction proposed by Agarwal.[4]

Our final comments with regard to the pressure buildup case are that this remains a topic for additional study. We believe that we have validated (at least conceptually) that the variable mobility model may represent the behavior of some cases of reservoir performance in gas condensate reservoirs. However, we believe that our concept of using a prescribed permeability profile may be inadequate — and that we must also employ a prescribed diffusivity profile. In short, we believe that we must consider the diffusive effects of the condensate bank in addition to the permeability (or effective/relative permeability) profile. Again, this is a recommendation for future work.

Summary and Conclusions

1. New Solution: We have proposed, developed, and verified new solutions (for pressure and the pressure derivative functions in terms of radial distance and time) for the case of a well producing at a constant flowrate from an infinite-acting radial flow system where the permeability varies in radial distance and time (see Eq. 1 for the model employed in this work).

   Eq. 1 is proposed based on observations of well performance behavior from numerical simulation of the gas phase for a radial gas condensate reservoir system.

   The relevant results in this work are given by Eqs. 3-5 and we note that Eq. 3 cannot be resolved beyond the integral formulation as presented. As such, all results for Eq. 3 are generated using numerical integration performed in *Mathematica*. The derivative formulations given by Eqs. 4 and 5 are closed form results — and are computationally efficient as well as convenient functional forms.

2. Comparison/Validation: The proposed solution is presented in comparison to numerical simulation results (for the $\partial p_D/\partial r_D$ formulation). The $\partial p_D/\partial t_D$ formulation is compared to the 2-zone radial composite model as well as simplified cases of "sealing faults" — the comparions indicate that the proposed solution does produce similar features and suggests the model would be an effective interpretation tool for well test analysis.

   Our presentation of the $p_{wD}(t_D)$ and $p_{wDd}(t_D)$ functions (which include wellbore storage and skin effects) indicate that the influence of the α (or α_D) parameter and the k_{min}/k_{max} ratio is substantive and unique for certain cases (*e.g.*, low values of C_D), while for higher values of C_D wellbore storage effects dominate the response. This is analogous to say, the case of well performance in a dual porosity/naturally fractured reservoir.

3. Pressure Buildup Case: This is a case for future investigation. The conventional pressure buildup formulation mimics the pressure drawdown case for the prescribed permeability profile. This is not an unexpected behavior for this formulation — and we suggest that this approach must be extended to include a variable "diffusivity" profile ($(\phi\mu_g c_g)/k_g$) as well as a variable mobility profile (k_g/μ_g) in order to capture the unique signature presented by the pressure buildup case.

Nomenclature

Field Variables (*Pressure, Formation, and Fluid Properties*)

B = Formation volume factor, RB/STB
c_g = Gas compressibility, psi^{-1}
c_t = Total compressibility, psi^{-1}
h = Net pay thickness, ft
k or k_g = Effective permeability to gas, md
k_{max} = Maximum effective permeability to gas, md
k_{min} = Minimum effective permeability to gas, md
p_i = Initial reservoir pressure, psia
p_{wf} = Flowing pressure, psia
p_{ws} = Shut-in pressure, psia
q = Flowrate, STB/D
q_{sf} = "Sandface" flowrate, STB/D
q_{sur} = "Surface" flowrate, STB/D
r_w = Wellbore radius, ft
r = Radial distance, ft
t = Time, hr
t_p = Production time, hr
Δt = Shut-in Time, hr
α = Scaling term for pressure behavior, (cp-psi^{-1})/md
ε = Boltzmann transform variable ($r^2/(4t)$)
μ = Viscosity, cp

DimensionlessVariables

C_D = Dimensionless wellbore storage coefficient
k_D = Dimensionless permeability function
p_D = Dimensionless pressure (generic)
p_{Ddr} = Dimensionless pressure derivative function in radial distance (Eq. 8)
p_{Ddt} = Dimensionless pressure derivative function in time (Eq. 7)
p_{sD} = p_D+s, Dimensionless pressure with skin effects
p_{wD} = Dimensionless pressure with wellbore storage and skin effects
p_{wDdt} = Dimensionless pressure derivative function in time including wellbore storage and skin effects
q_{Dwbs} = Dimensionless flowrate for wellbore storage
r_D = Dimensionless radius
t_D = Dimensionless time
t_{pD} = Dimensionless production time
Δt_D = Dimensionless shut-in time
ε_D = Dimensionless Boltzmann transform variable
a_D = Dimensionless empirical scaling term for pressure behavior
s = Skin factor, dimensionless

References

1. Roussenac, B.: *Gas Condensate Well Analysis*, M.S. Thesis, Stanford University, June 2001.
2. *Mathematica* (software) Ver. 4.1, Wolfram Research, Champaign-Urbana, IL (2001).
3. Blasingame, T.A., Johnston, J.L., and Lee, W.J.: "Advances in the Use of Convolution Methods in Well Test Analysis," paper SPE 21826 presented at the 1991 Joint Rocky Mountain Regional/Low Permeability Reservoirs.
4. Agarwal, R.G.: "A New Method to Account for Producing Time Effects When Drawdown Type Curves are used to Analyze Pressure Buildup and other Well Test Data, paper SPE 9289 presented at the 1980 SPE Annual Technical Conference and Exhibition, Dallas, TX, 21-24 September 1980.

Appendix A — Derivation of the Pressure Derivative Functions with Respect to Time and Radius for the Case of a Radially-Varying Permeability Profile (Equivalent Liquid Case)

In this Appendix, we derive two expressions for the pressure derivative (time and radial distance formulations) that consider the changing effective (or relative) permeability of the retrograde gas as condensate evolves with decreasing pressure.

This derivation begins with the base diffusivity equation — *i.e.*, the partial differential equation which describes the flow of a single phase fluid in a porous medium with respect to time and distance. The effective permeability to gas in such cases will not be constant, but is dependent on the PVT and rock-fluid properties. The primary contribution of this work is the development of a closed form analytical solution for the case of a radially varying mobility (or effective permeability) function in a reservoir system. The subordinate contribution (which is, in some ways, more important than the solution) is our proposal of a simple functional relationship to represent the time and space-dependency of the gas mobility (or permeability) function.

The base form of the diffusivity equation which considers a varying permeability with respect to radius is given as:

$$\frac{1}{r}\frac{\partial}{\partial r}\left[kr\frac{\partial p}{\partial r}\right]=\frac{1}{0.0002637}\phi\mu c_t\frac{\partial p}{\partial t}\ \text{(Field units)...}\ \text{(A.1)}$$

As mentioned above, we have proposed a general model for the behavior of the permeability to gas as a function of time

and radius. Our proposed model is given in its 2 most basic forms as:

$$k = k_{min} + (k_{max} - k_{min})\left[1 - \exp\left[\frac{-1}{\alpha}\frac{r^2}{t}\right]\right] \quad \text{(A.2a)}$$

$$k = k_{max} - (k_{max} - k_{min})\exp\left[\frac{-1}{\alpha}\frac{r^2}{t}\right] \quad \text{(A.2b)}$$

We note that the α-parameter in Eqs. A.2a and A.2b is an empirical constant, most likely related to the PVT characteristics of the reservoir fluid, as well as the rock-fluid properties. Our goal is not to assess the nature of the α-parameter, but rather, to use this as a mechanism to represent a complex process with a simple model. Eq. A.2b is the primary form used in this Appendix, and we will note that Eqs. A.2a and A.2b have been validated conceptually via comparison with simulated performance for a gas condensate reservoir system.

We consider the Boltzmann transform, which allows us to relate dimensionless time and distance:

$$\varepsilon_D = \frac{r_D^2}{4t_D} \quad \text{(A.3)}$$

$$\frac{r^2}{\alpha t} = \frac{r_D^2}{\alpha_D t_D} \quad \text{(A.4)}$$

Substituting Eqs. A.3 and A.4 into Eq. A.2b yields:

$$k = k_{max} - (k_{max} - k_{min})\exp\left[\frac{-4}{\alpha_D}\varepsilon_D\right] \quad \text{(A.5)}$$

Defining a "dimensionless" permeability, k_D, we have:

$$k_D = k/k_{max} \quad \text{(A.6)}$$

or, solving Eq. A.6 for the permeability, we obtain:

$$k = k_{max} k_D$$

We note that we will use the terms "permeability" and "effective permeability" interchangeably in this derivation — however, the variable in question is always *effective* permeability.

Substituting the definition of "dimensionless" permeability (*i.e.*, Eq. A.6) into Eq. A.5 gives us:

$$k_D = 1 - \left[1 - \frac{k_{\min}}{k_{\max}}\right]\exp\left[\frac{-4}{\alpha_D}\varepsilon_D\right] \quad \text{(A.7)}$$

We need to transform Eq. A.1 into dimensionless form — hence, we state the dimensionless variables used in this work are as follows: (Field units formulation)

Dimensionless Pressure:

$$p_D = \frac{1}{141.2}\frac{k_{max}h}{qB\mu}(p_i - p) \quad \text{(A.8)}$$

Dimensionless Time:

$$t_D = 0.0002637\frac{k_{max}}{\phi\mu c_t r_w^2}t \quad \text{(A.9)}$$

Dimensionless Radius:

$$r_D = \frac{r}{r_w} \quad \text{(A.10)}$$

Substituting Eqs A.9 and A.10 into Eq. A.4 and solving for the α_D parameter, we have:

$$\alpha_D = \frac{r_D^2}{r^2}\frac{t}{t_D}\alpha = \frac{1}{0.0002637}\frac{1}{r_w^2}\frac{\phi\mu c_t r_w^2}{k_{max}}\alpha$$

Or,

$$\alpha_D = \frac{1}{0.0002637}\frac{\phi\mu c_t}{k_{max}}\alpha \quad \text{(A.11)}$$

From Eq. A.11 we note that the α-parameter has the units of inverse diffusivity (*i.e.*, diffusivity ($k/(\phi\mu c_t)$) has the units of (md/(cp-psi^{-1}) — field units formulation) — therefore, α has the units of (cp-psi^{-1})/md. Physically, we assign the properties of the fluid and rock-fluid interaction to the α-parameter — however, we consider α to be an empirical parameter, and, as such, we should not attempt to quantify the components of α, but rather, we should simply use α to qualify the influence of the fluid on the permeability profile.

Substituting Eqs A.6, A.8-.10 into Eq. A.1 and rearranging yields the diffusivity equation in dimensionless form:

$$\frac{1}{r_D}\frac{\partial}{\partial r_D}\left[k_D r_D \frac{\partial p_D}{\partial r_D}\right] = \frac{\partial p_D}{\partial t_D} \quad \text{(A.12)}$$

We note that for the case where $k = k_{max}$, Eq. A.12 reverts to the conventional diffusivity equation for a constant permeability. We also note that we have assumed a slightly compressible fluid (*i.e.*, a liquid) in the derivation of the diffusivity equation for radial flow (*i.e.*, Eq. A.1). The assumption of a "liquid" may seem incompatible with the concept of a gas case — however, we are deriving a formulation for a "liquid" that will, in turn, be used for gases where the conventional gas pseudofunctions will be employed (*i.e.*, pseudopressure and pseudotime). Simply put, this case represents an "equivalent" liquid, modifications will be addressed using pseudofunctions that "convert" the case in question to the "equivalent" liquid case.

Utilizing the Boltzmann transform we derive a relationship for pressure with respect to time and radius which includes the prescribed varying permeability model (*i.e.*, Eq. A.2 or A.7).

For convenience, we define the constants *a* and *b* as follows:

$$a = (1 - k_{min}/k_{max}) \quad \text{(A.13)}$$

$$b = \frac{4}{\alpha_D} \quad \text{(A.14)}$$

Substituting Eqs. A.13 and A.14 into Eq. A.7 yields:

$$k_D = 1 - a\,exp[-b\varepsilon_D] \quad \text{(A.15)}$$

Applying the product rule to the left-hand-side (LHS) of Eq. A.12 we have:

$$\frac{1}{r_D}\left[r_D\frac{\partial p_D}{\partial r_D}\frac{\partial k_D}{\partial r_D} + k_D\frac{\partial p_D}{\partial r_D}\frac{\partial r_D}{\partial r_D} + k_D r_D\frac{\partial}{\partial r_D}\left[\frac{\partial p_D}{\partial r_D}\right]\right] = \frac{\partial p_D}{\partial t_D}$$

Multiplying through the left-hand-side by $1/r_D$ gives:

$$\frac{\partial k_D}{\partial r_D}\frac{\partial p_D}{\partial r_D} + \frac{k_D}{r_D}\frac{\partial p_D}{\partial r_D} + k_D\frac{\partial}{\partial r_D}\left[\frac{\partial p_D}{\partial r_D}\right] = \frac{\partial p_D}{\partial t_D}$$

Collecting like terms and consolidating the k_D terms:

$$\frac{\partial k_D}{\partial r_D}\frac{\partial p_D}{\partial r_D}+k_D\left[\frac{\partial}{\partial r_D}\frac{\partial p_D}{\partial r_D}+\frac{1}{r_D}\frac{\partial p_D}{\partial r_D}\right]=\frac{\partial p_D}{\partial t_D} \quad \text{..... (A.16)}$$

Utilizing the Boltzmann variable, ε_D, to transform Eq. A.16 from r_D and t_D into ε_D, we have:

$$\frac{d^2 p_D}{d\varepsilon_D^2}+\left[\frac{1}{\varepsilon_D}+\frac{1}{k_D}\left[1+\frac{dk_D}{d\varepsilon_D}\right]\right]\frac{dp_D}{d\varepsilon_D}=0 \quad \text{..... (A.17)}$$

At this point we recognize that Eq. A.17 is the fundamental governing relation for fluid flow in our system where the mobility/permeability function is permitted to vary as a function of time and distance. Eq. A.17 is a completely general result — no assumptions have been made at this point.

Our goal is to solve Eq. A.17 for an appropriate set of initial and boundary conditions. The particular case where the Boltzmann transform applies is the case of a uniform initial pressure profile in the reservoir (*i.e.*, $p_D(r_D,t_D=0)=0$) and the case of an "infinite-acting" outer boundary (*i.e.*, $p_D(r_D\rightarrow\infty,t_D)=0$).

Recalling the definition of the Boltzmann transform variable, ε_D, we have:

$$\varepsilon_D=\frac{r_D^2}{4t_D} \quad \text{..... (A.3)}$$

The initial and outer boundary conditions are expressed in terms of r_D, t_D, and ε_D as follows:

Initial Condition:

$$p_D(r_D,t_D\le 0)=0$$
$$\text{for } t_D\rightarrow 0,\varepsilon_D\rightarrow\infty$$
$$p_D(\varepsilon_D\rightarrow\infty)=0$$

Outer Boundary Condition:

$$p_D(r_D\rightarrow\infty,t_D)=0$$
$$\text{for } r_D\rightarrow\infty,\varepsilon_D\rightarrow\infty$$
$$p_D(\varepsilon_D\rightarrow\infty)=0$$

We note that in using the Boltzmann transformation, the initial and outer boundary conditions collapse to a single relation:

$$p_D(\varepsilon_D\rightarrow\infty)=0 \quad \text{..... (A.18)}$$

This result is a unique product of the Boltzmann transformation — *for this particular case*. We will proceed with this result and next we consider the case of a constant flowrate at the well.

Inner Boundary Condition: (Constant Rate)

$$q=\frac{1}{141.2}\frac{kh}{B\mu}r\frac{\partial p}{\partial r} \quad \text{..... (A.19)}$$

Where Eq. A.19 is written directly from Darcy's law for a radial flow geometry. Isolating the $r(\partial p/\partial r)$ term, we have:

$$r\frac{\partial p}{\partial r}=141.2\frac{qB\mu}{kh} \quad \text{..... (A.20)}$$

Substituting the definitions of dimensionless pressure, radius, and permeability (*i.e.*, Eqs. A.6, A.8, and A.11) into Eq. A.20, and rearranging gives us the following result for the behavior at r=0: (*i.e.*, the "line source" formulation)

$$\left[r_D\frac{\partial p_D}{\partial r_D}\right]_{r_D=0}=-\frac{1}{k_D} \quad \text{..... (A.21)}$$

Transforming Eq. A.21 using the Boltzmann variable, ε_D, gives us:

$$\left[\varepsilon_D\frac{dp_D}{d\varepsilon_D}\right]_{\varepsilon_D\rightarrow 0}=-\frac{1}{2}\frac{1}{k_D} \quad \text{..... (A.22)}$$

In order to develop a solution for Eq. A.17 we will utilize a "variable of transformation" that reduces the differential equation to a more convenient form. At this point we note that Eqs. A.17, A.18, and A.22 are only a function of the Boltzmann transform variable, ε_D. As Eq. A.17 is a second order ordinary differential equation, we can surmise that a solution can be obtained by twice integrating this differential equation (analogous to the homogeneous reservoir case). This will be our path, but we will also use a variable of transformation to reduce the complexity for the integration of Eq. A.17.

Our "variable of transformation," v, is given by:

$$v=\frac{dp_D}{d\varepsilon_D}$$

where

$$\frac{dv}{d\varepsilon_D}=\frac{d^2 p_D}{d\varepsilon_D^2}$$

Making these substitutions into Eq. A.17 gives the following "compact form" of the differential equation — we then will solve this relation by integration for the v-variable.

$$\frac{dv}{d\varepsilon_D}+\left[\frac{1}{\varepsilon_D}+\frac{1}{k_D}\left[1+\frac{dk_D}{d\varepsilon_D}\right]\right]v=0 \quad \text{..... (A.23)}$$

Using Eq. A.15 in the $\frac{1}{k_D}\left[1+\frac{dk_D}{d\varepsilon_D}\right]$ term from Eq. A.23:

$$\frac{1}{k_D}\left[1+\frac{dk_D}{d\varepsilon_D}\right]=\frac{1+ab\,exp[-b\varepsilon_D]}{1-a\,exp[-b\varepsilon_D]} \quad \text{..... (A.24)}$$

Substituting Eq.A.24 into Eq. A.23 yields,

$$\frac{dv}{d\varepsilon_D}+\left[\frac{1}{\varepsilon_D}+\frac{1+ab\,exp[-b\varepsilon_D]}{1-a\,exp[-b\varepsilon_D]}\right]v=0$$

Isolating/separating the relevant terms we have:

$$\frac{1}{v}dv=-\left[\frac{1}{\varepsilon_D}+\frac{1+ab\,exp[-b\varepsilon_D]}{1-a\,exp[-b\varepsilon_D]}\right]d\varepsilon_D \quad \text{..... (A.25)}$$

Setting up the integration of Eq. A.26 gives us:

$$\int\frac{1}{v}dv=-\int\left[\frac{1}{\varepsilon_D}+\frac{1+ab\,exp[-b\varepsilon_D]}{1-a\,exp[-b\varepsilon_D]}\right]d\varepsilon_D$$

Expanding the right-hand-side integral gives:

$$\int\frac{1}{v}dv=-\int\frac{1}{\varepsilon_D}d\varepsilon_D-\int\frac{1+ab\,exp[-b\varepsilon_D]}{1-a\,exp[-b\varepsilon_D]}d\varepsilon_D$$

Completing the integration, we have:

$$\ln[v]=-\ln[\varepsilon_D]-\int\frac{1+ab\,exp[-b\varepsilon_D]}{1-a\,exp[-b\varepsilon_D]}d\varepsilon_D+\beta \quad \text{.. (A.26)}$$

We note that the β-term in Eq. A.26 is a constant of integration which results from the indefinite integration. The integral that can not be resolved directly in Eq. 26 must be addressed using tables of integrals, substitution methods, or a symbolic integration product (in this case, we used *Mathematica* (ref. 2)).

From *Mathematica* we obtained the following result for the remaining integral:

$$I = \int \frac{1+ab\,exp[-b\varepsilon_D]}{1-a\,exp[-b\varepsilon_D]}d\varepsilon_D = -\left[\frac{(1+b)}{b}\ln[e^{-b\varepsilon_D}-a]-b\varepsilon_D\right]$$

Substituting this result into the solution, we have:

$$\ln[v] = -\ln[\varepsilon_D]-\left[\frac{(1+b)}{b}\ln[e^{-b\varepsilon_D}-a]-b\varepsilon_D\right]+\beta$$

Exponentiating the solution, we obtain:

$$v = \frac{\exp[\beta]}{\varepsilon_D}\exp\left[-\left[\frac{(1+b)}{b}\ln[e^{-b\varepsilon_D}-a]-b\varepsilon_D\right]\right]$$

Defining our constant of integration as c_1=exp[β], and substituting this result into the solution, along with the definition v=$dp_D/d\varepsilon_D$, we have:

$$\frac{dp_D}{d\varepsilon_D} = c_1\frac{1}{\varepsilon_D}\exp\left[-\frac{(1+b)}{b}\ln[e^{-b\varepsilon_D}-a]+b\varepsilon_D\right] \quad \text{..... (A.27)}$$

Our next task is to determine the constant of integration, c_1, where this can be accomplished using the inner boundary condition (*i.e.*, Eq., A.22). Multiplying through Eq. A.27 by the Boltzmann transform variable, ε_D, we have:

$$\varepsilon_D\frac{dp_D}{d\varepsilon_D} = c_1\exp\left[-\left[\frac{(1+b)}{b}\ln[e^{-b\varepsilon_D}-a]-b\varepsilon_D\right]\right] \quad \text{..... (A.28)}$$

Solving for the constant of integration, c_1, we have:

$$c_1 = -\frac{1}{2}(1-a)^{\frac{1}{b}} \quad \text{..... (A.29)}$$

Substitution of the constant of integration, c_1, (Eq. A.29) into the general solution (Eq. A.28) gives:

$$\frac{dp_D}{d\varepsilon_D} = -\frac{1}{2}(1-a)^{\frac{1}{b}}\frac{1}{\varepsilon_D}\exp\left[-\frac{(1+b)}{b}\ln[e^{-b\varepsilon_D}-a]+b\varepsilon_D\right] \quad \text{..... (A.30)}$$

Definite integration of Eq. A.30 (using this initial condition) yields the solution in terms of $p_D(\varepsilon_D)$ — this result is given as:

$$p_D = -\frac{1}{2}(1-a)^{\frac{1}{b}}\int_{\infty}^{\varepsilon_D}\left[\frac{1}{\varepsilon_D}\exp\left[-\frac{(1+b)}{b}\ln[e^{-b\varepsilon_D}-a]+b\varepsilon_D\right]\right]d\varepsilon_D \quad \text{..... (A.31)}$$

Reversing the limits of integration in Eq. A.37 eliminates the (-) sign and puts the result into a more traditional form.

$$p_D = \frac{1}{2}(1-a)^{\frac{1}{b}}\int_{\varepsilon_D}^{\infty}\left[\frac{1}{\varepsilon_D}\exp\left[-\frac{(1+b)}{b}\ln[e^{-b\varepsilon_D}-a]+b\varepsilon_D\right]\right]d\varepsilon_D \quad \text{..... (A.32)}$$

Unfortunately, Eq. A.32 can only be integrated numerically — we have also employed *Mathematica* as the mechanism to compute the numerical integration of Eq. A.32 for the cases considered in this work.

Solving Eq. A.32 for the time and radial distance derivative forms, we have:

$$t_D\frac{\partial p_D}{\partial t_D} = \frac{1}{2}(1-a)^{\frac{1}{b}}\exp\left[-\frac{(1+b)}{b}\ln[e^{-b\frac{r_D^2}{4t_D}}-a]+b\frac{r_D^2}{4t_D}\right] \quad \text{..... (A.33)}$$

And,

$$-r_D\frac{\partial p_D}{\partial r_D} = (1-a)^{\frac{1}{b}}\exp\left[-\frac{(1+b)}{b}\ln[e^{-b\frac{r_D^2}{4t_D}}-a]+b\frac{r_D^2}{4t_D}\right] \quad \text{..... (A.34)}$$

Where we recognize that the right-hand-sides (RHS) of Eqs. A.33 and A.34 are identical (except for the 1/2 multiplier in Eq. A.33) — as such, equating Eqs. A.33 and A.34 gives the following identity:

$$2t_D\frac{\partial p_D}{\partial t_D} = -r_D\frac{\partial p_D}{\partial r_D} \quad \text{..... (A.35)}$$

We note that the identity given by Eq. A.35 is also obtained for the "homogeneous" case where k_D = 1. In fact, for the case of k_D = 1, the entire sequence of results reverts to the "traditional" line source solution for a homogeneous, infinite-acting reservoir. We also note that Eq. A.34 is typically applied as the absolute value of this result for comparative/illustrative plots (obviously the $\partial p_D/\partial r_D$ term is negative).

Appendix B — An Approximate Technique for the Direct Addition of Wellbore Storage and Skin Effects

In this Appendix, we present a simple, approximate technique for adding wellbore storage to dimensionless pressure solutions. This result is taken from Blasingame, *et al.*[3]

The required result from (ref. 3) is given as:

$$p_{wD} = \frac{\psi}{\omega}(1-\exp[-\omega t_D])+\frac{\theta}{\omega^2}(\exp[-\omega t_D]+\omega t_D-1) \quad \text{..... (B.1)}$$

Where the ω, θ, and ψ parameters in Eq. B.1 are given by:

$$\omega = \frac{1+C_D\hat{b}}{C_D\hat{a}} \quad \text{..... (B.2)}$$

$$\psi = \frac{1}{C_D} \quad \text{(B.3)}$$

$$\theta = \frac{\hat{b}}{\hat{a}C_D} \quad \text{(B.4)}$$

Where the $\hat{a}$ and $\hat{b}$ parameters in Eqs. B.2 and B.4 are given by:

$$\hat{a} = p_{sD} - p_{sDd} \quad \text{(B.5)}$$

$$\hat{b} = \frac{dp_{sD}}{dt_D} \quad \text{(B.6)}$$

And,

$$p_{sDd} = t_D \frac{dp_{sD}}{dt_D} \quad \text{(B.7)}$$

Eq. B.1 should provide results which are accurate to within 1-2 percent of the exact solution — for the p_{wD} and the p_{wDd} functions (where $p_{wDd}=t_D(dp_{wD}/dt_D)$).

Appendix C — A Quadratic Formula for Numerical Differentiation

Presuming a general quadratic polynomial, we have:

$$y = a_0 + a_1 t + a_2 t^2 \quad \text{(C.1)}$$

The coefficients of an interpolating LaGrange collocation polynomial are stated as follows:

$$c_0 = y(t_i) \quad \text{(C.2)}$$

$$c_1 = \frac{y(t_{i-1}) - y(t_i)}{t_{i-1} - t_i} \quad \text{(C.3)}$$

$$c_2 = \frac{y(t_{i-2}) - c_0 - c_1(t_{i-2} - t_i)}{(t_{i-2} - t_i)(t_{i-2} - t_{i-1})} \quad \text{(C.4)}$$

Where we note that we have used a "backward" sampling for the coefficients (*i.e.*, in terms of t_i, t_{i-1}, and t_{i-2}) — this is for convenience in our present work. Alternatively, we could use forward or central sampling with no loss in generality.

The a_0, a_1, and a_2 coefficients for Eq. C.1 are defined in terms of the coefficients of the collocation polynomial as follows:

$$a_0 = c_0 - c_1 t_i + c_2 t_i t_{i-1} \quad \text{(C.5)}$$

$$a_1 = c_1 - c_2(t_i + t_{i-1}) \quad \text{(C.6)}$$

$$a_2 = c_2 \quad \text{(C.7)}$$

The derivative of Eq. C.1 is:

$$\frac{dy}{dt} = a_1 + 2a_2 t \quad \text{(C.8)}$$

Given a table of t and $y(t)$ values, Eqs. C.2-C.7 are used to compute the required coefficients. Eq. C.8 is used to compute the desired derivative.

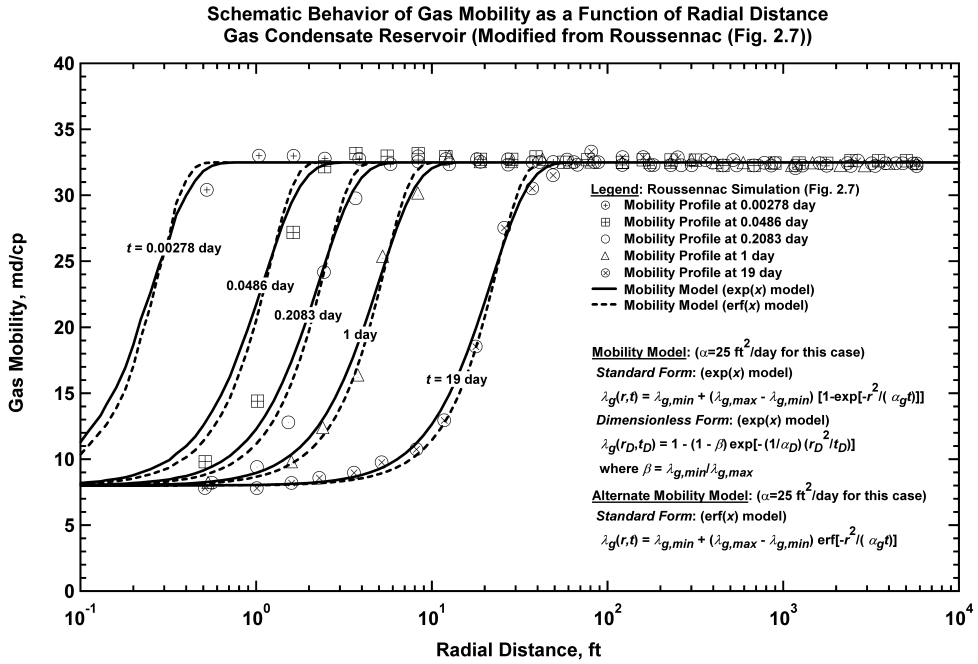

Figure 1 – Gas mobility profiles for a gas condensate reservoir system (as a function of time and radius) (adapted from Roussennac[1]) — note the comparison of the simulated performance and the proposed models (*i.e.*, the exp(x) and the erf (x) mobility models).

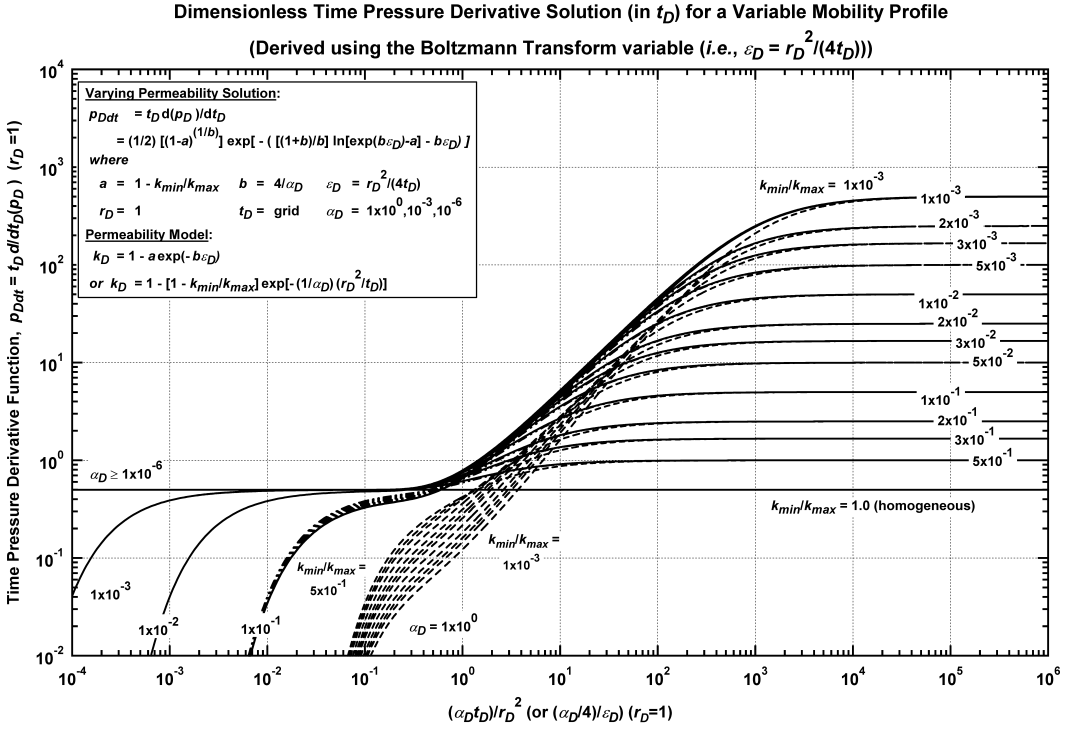

Figure 2 – "Type curve" representation of the new model ($t_D(\partial p_D/\partial t_D)$ formulation (Eq. 4)). Solution is plotted versus the inverse of the modified Boltzmann transform variable ($(\alpha_D t_D)/r_D^2$).

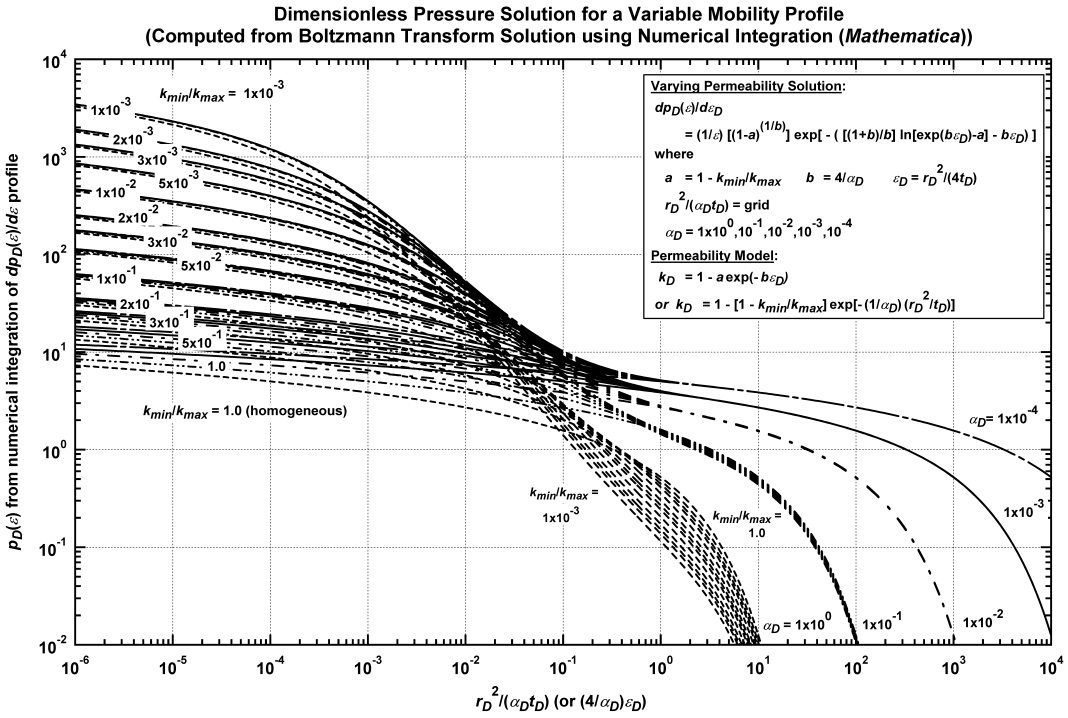

Figure 3a – "Type curve" representation of the new model ($p_D(\varepsilon_D)$ formulation (Eq. 3)). Solution is plotted versus the modified Boltzmann transform variable ($(\alpha_D t_D)/r_D^2$).

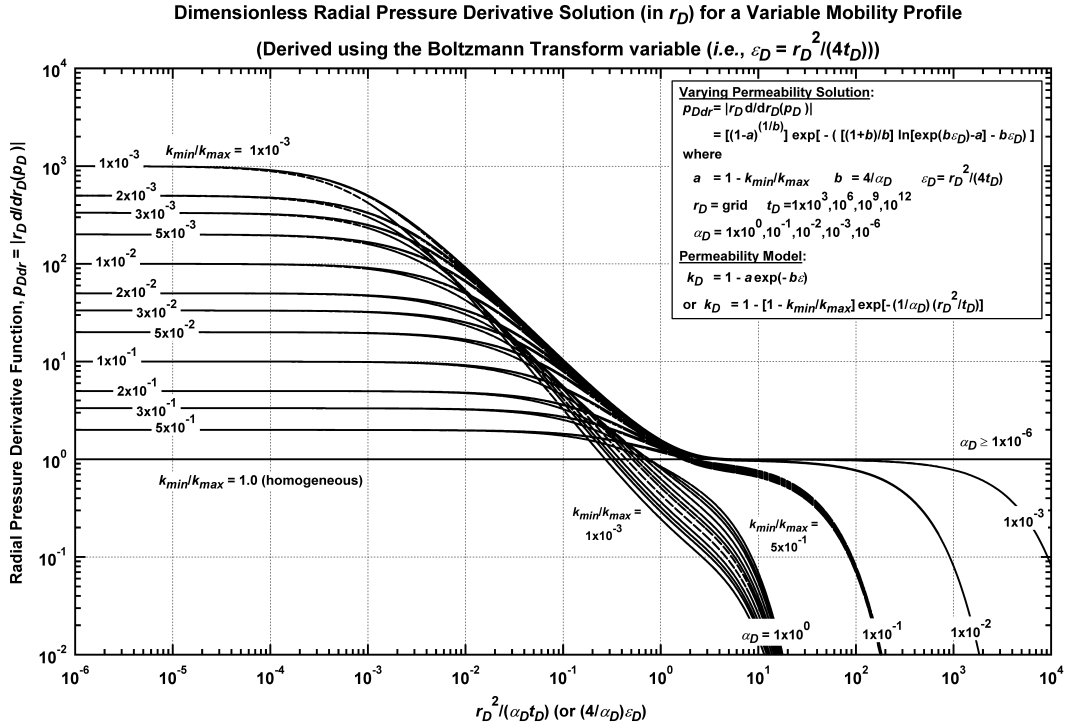

Figure 3b – "Type curve" representation of the new model ($|r_D(\partial p_D/\partial t_D)|$ formulation (Eq. 5)). Solution is plotted versus the modified Boltzmann transform variable ($(\alpha_D t_D)/r_D^2$).

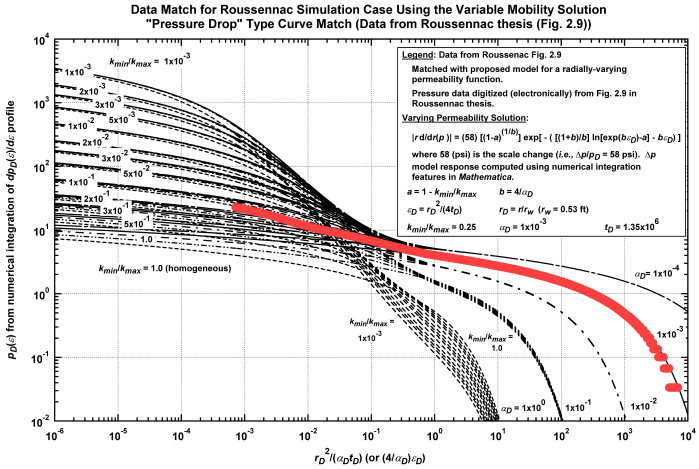

Figure 4a – Match of Roussenac data (digitized) and the new variable mobility model (type curve match) — $p_D(\varepsilon_D)$ versus $(\alpha_D t_D)/r_D^2$ format.

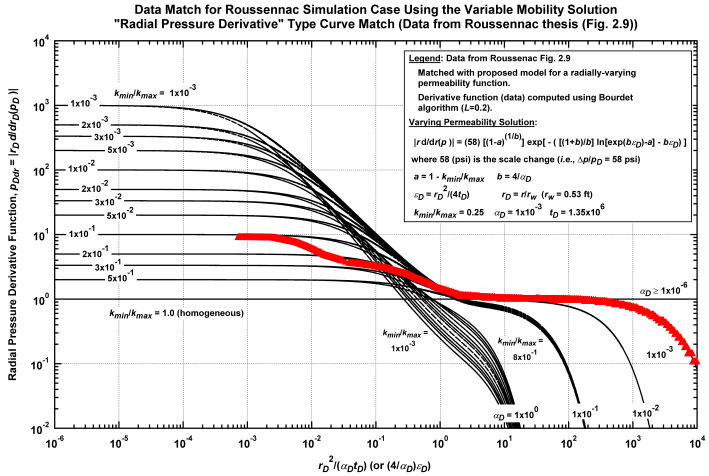

Figure 4b – Match of Roussenac data (digitized) and the new variable mobility model (type curve match) — $|r_D(\partial p_D/\partial t_D)|$ versus $(\alpha_D t_D)/r_D^2$ format.

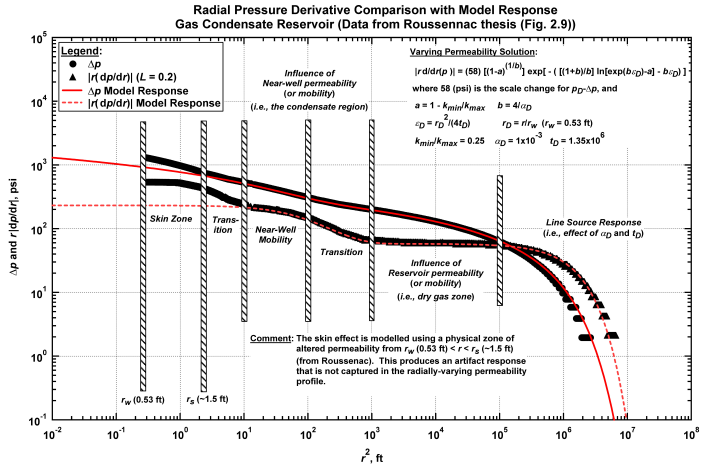

Figure 5 – Match of Roussenac data (digitized) and the new variable mobility model (data/model match) — Δp and $r|dp/dr|$ versus r^2 format. Note the excellent match of the data and model functions throughout the reservoir — except for the "skin zone" near the wellbore.

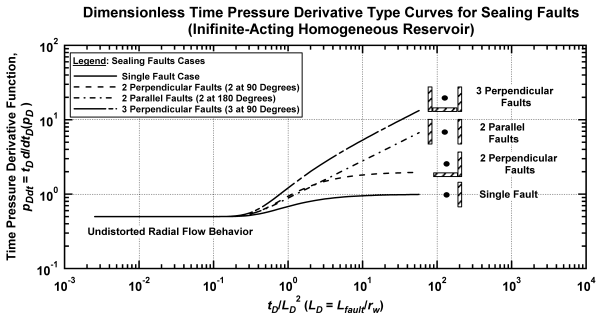

Figure 6 – Pressure derivative type curve for a vertical well producing at a constant rate near a sealing fault in a homogeneous, infinite-acting reservoir.

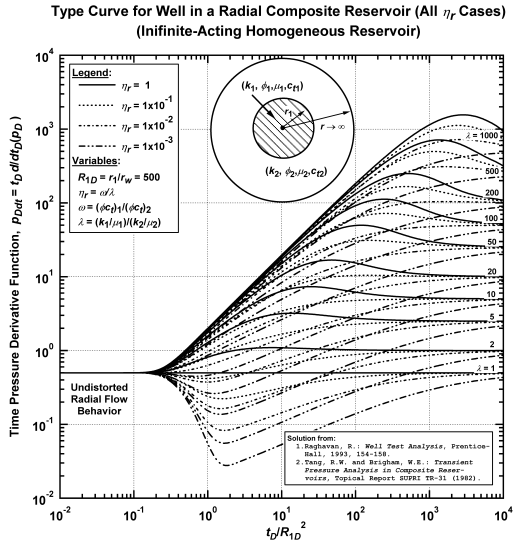

Figure 7 – Pressure derivative type curve for a vertical well producing at a constant rate in a composite radial system, various mobility (λ)/storativity (ω) cases.

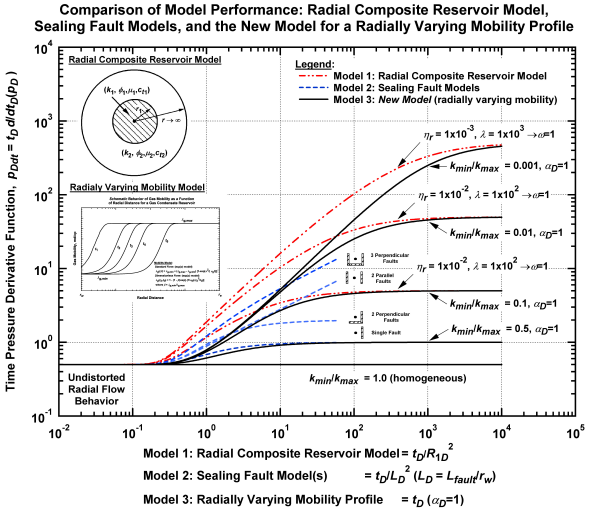

Figure 8 – Combined pressure derivative type curve for the following cases: sealing faults, a single radial composite region, and the proposed model for a radially-varying mobility profile.

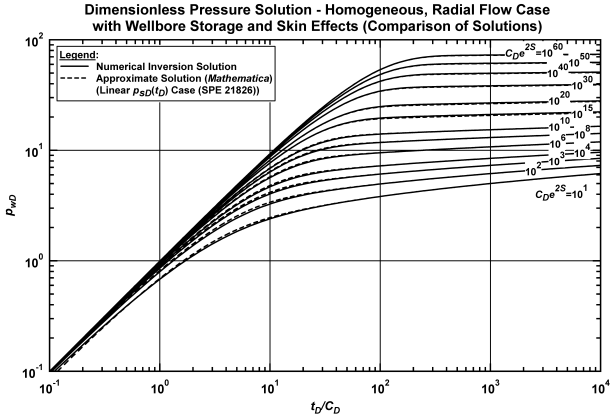

Figure 9a – Dimensionless pressure type curve for radial flow behavior including wellbore storage and skin effects (p_{wD} versus t_D/C_D format). This plot presents a comparison of the solution generated using numerical inversion (as a surrogate for the exact solution) and the approximate solution technique proposed in ref. 3 and generated using *Mathematica*.

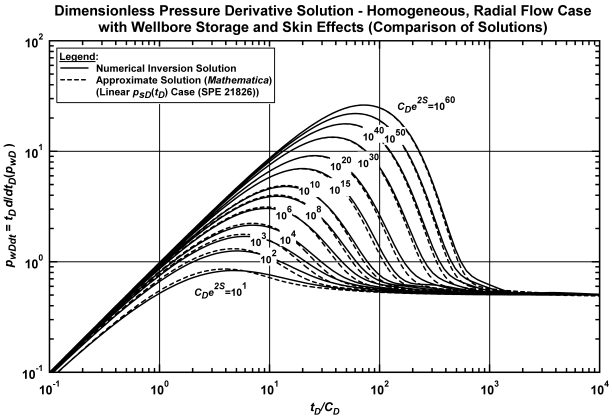

Figure 9b – Dimensionless pressure derivative type curve for radial flow behavior including wellbore storage and skin effects (p_{wD}' versus t_D/C_D format). This plot presents a comparison of the solution generated using numerical inversion (as a surrogate for the exact solution) and the approximate solution technique proposed in ref. 3 and generated using *Mathematica*.

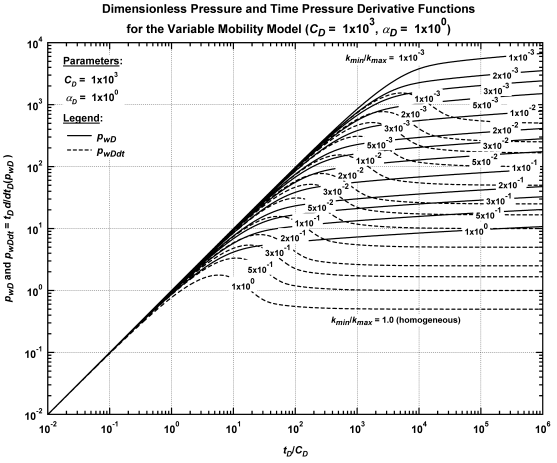

Figure 10a – Type curve plot (p_{wD} and p_{wD}' versus t_D/C_D) — C_D = 1x10^3, α_D = 1x10^0, various k_{min}/k_{max} cases.

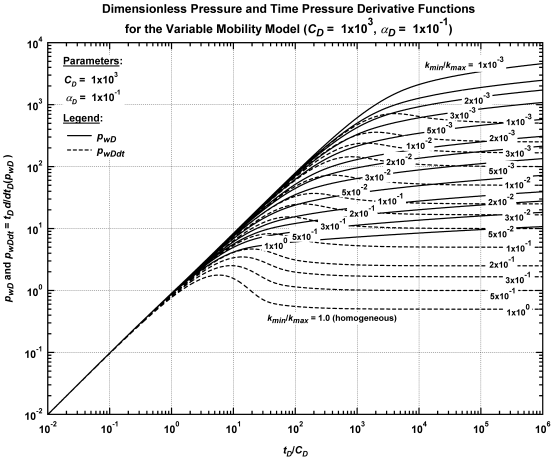

Figure 10b – Type curve plot (p_{wD} and p_{wD}' versus t_D/C_D) — C_D = 1x10^3, α_D = 1x10^{-1}, various k_{min}/k_{max} cases.

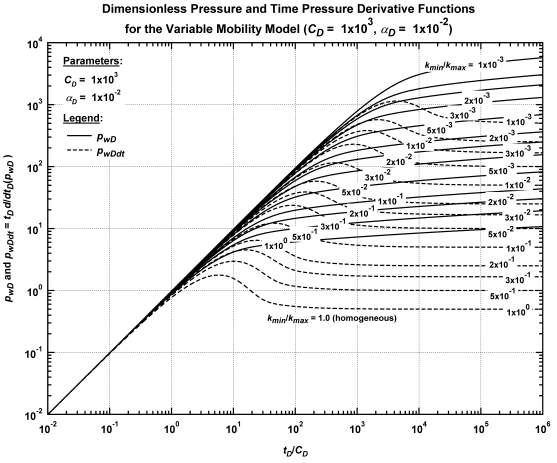

Figure 10c – Type curve plot (p_{wD} and p_{wD}' versus t_D/C_D) — C_D = 1x10^3, α_D = 1x10^{-2}, various k_{min}/k_{max} cases.

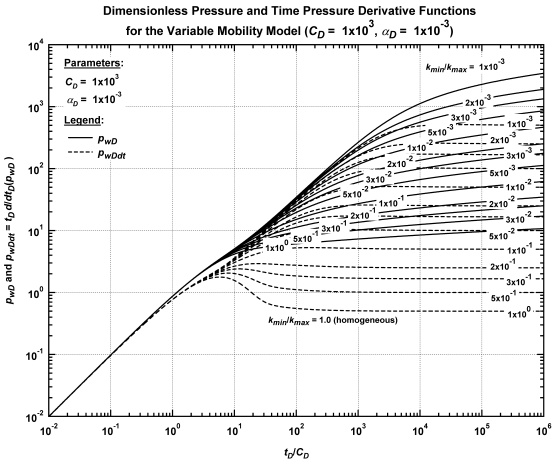

Figure 10d – Type curve plot (p_{wD} and p_{wD}' versus t_D/C_D) — C_D = 1x10^3, α_D = 1x10^{-3}, various k_{min}/k_{max} cases.

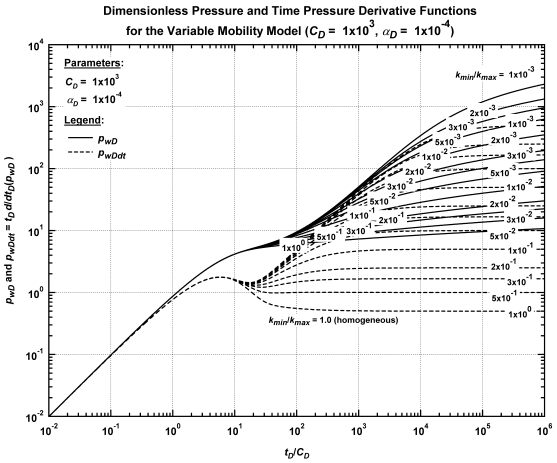

Figure 10e – Type curve plot (p_{wD} and p_{wD}' versus t_D/C_D) — C_D = 1x10^3, α_D = 1x10^{-4}, various k_{min}/k_{max} cases.

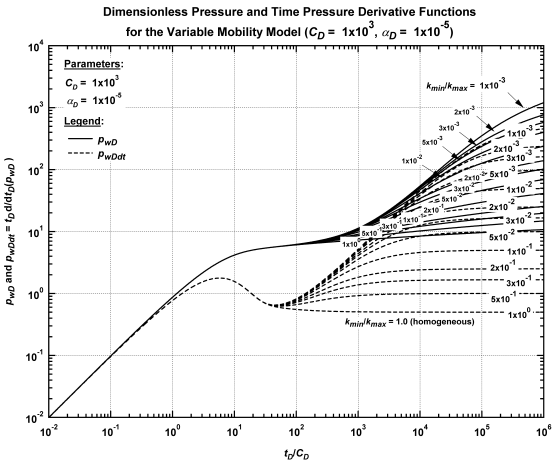

Figure 10f – Type curve plot (p_{wD} and p_{wD}' versus t_D/C_D) — C_D = 1x10^3, α_D = 1x10^{-5}, various k_{min}/k_{max} cases.

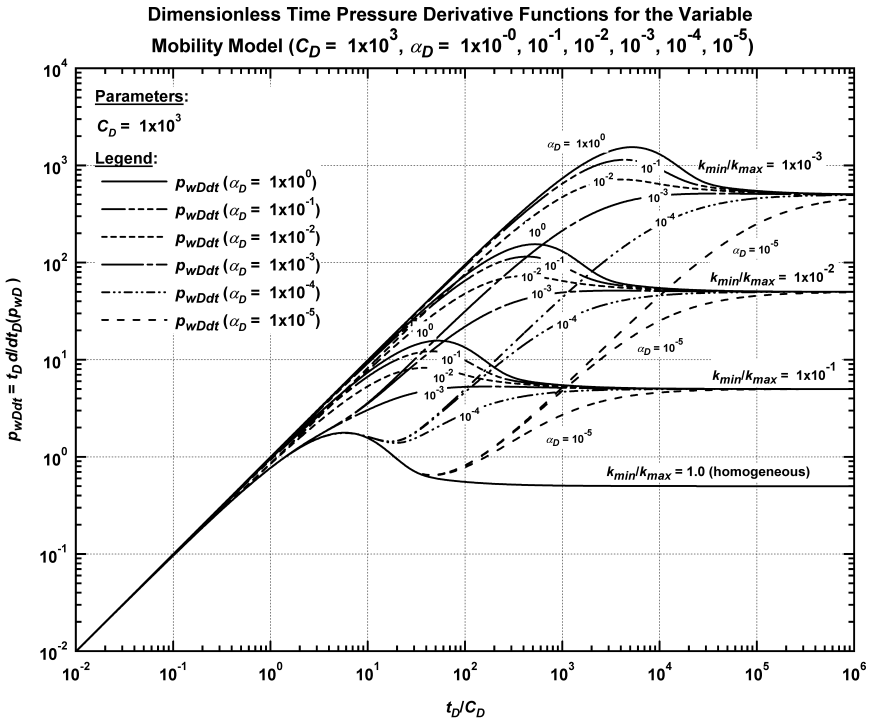

Figure 11– Drawdown type curve plot (p_{wD}' versus t_D/C_D) — C_D = 1x10^3, α_D = 1x10^0, 10^{-1}, 10^{-2}, 10^{-3}, 10^{-4}, 10^{-5}, various k_{min}/k_{max} = 1x10^0, 10^{-1}, 10^{-2}, 10^{-3}. Note the unique influence of both the α_D and the k_{min}/k_{max} parameters — this comparison indicates that the proposed model has a strong characteristic behavior for C_D = 1x10^3.

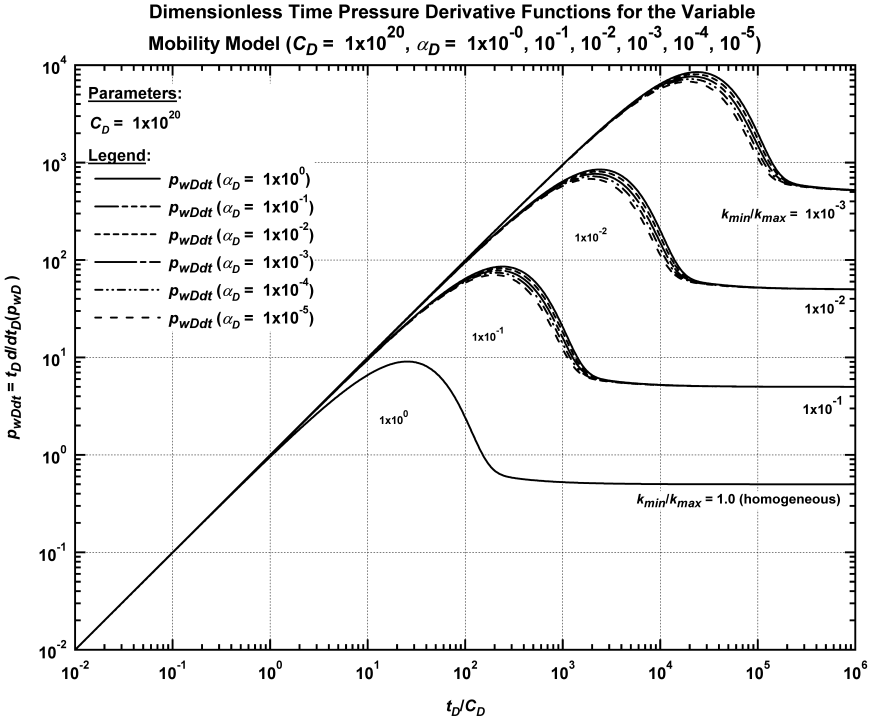

Figure 12– Drawdown type curve plot (p_{wD}' versus t_D/C_D) — C_D = 1x10^{20}, α_D = 1x10^0, 10^{-1}, 10^{-2}, 10^{-3}, 10^{-4}, 10^{-5}, various k_{min}/k_{max} = 1x10^0, 10^{-1}, 10^{-2}, 10^{-3}. Note that the α_D parameter does not exert a strong influence on the characteristic behavior for C_D = 1x10^{20}.

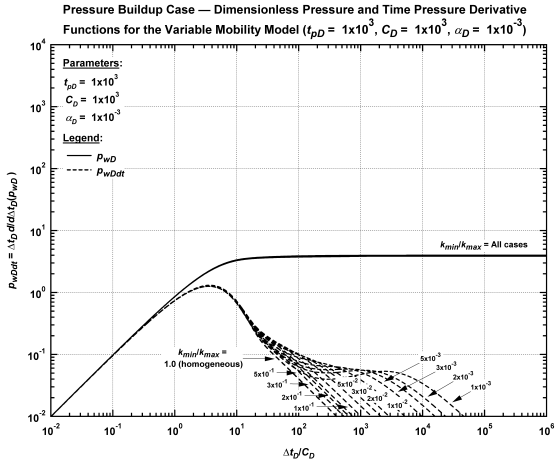

Figure 13a – Type curve plot (p_{wD} and p_{wD}' versus $\Delta t_D/C_D$) — t_{pD} = 1x10^3, C_D = 1x10^3, α_D = 1x10^{-3}, various k_{min}/k_{max} cases.

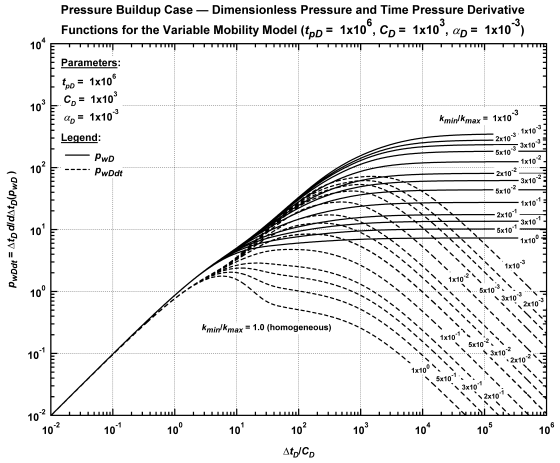

Figure 13b – Type curve plot (p_{wD} and p_{wD}' versus $\Delta t_D/C_D$) — t_{pD} = 1x10^6, C_D = 1x10^3, α_D = 1x10^{-3}, various k_{min}/k_{max} cases.

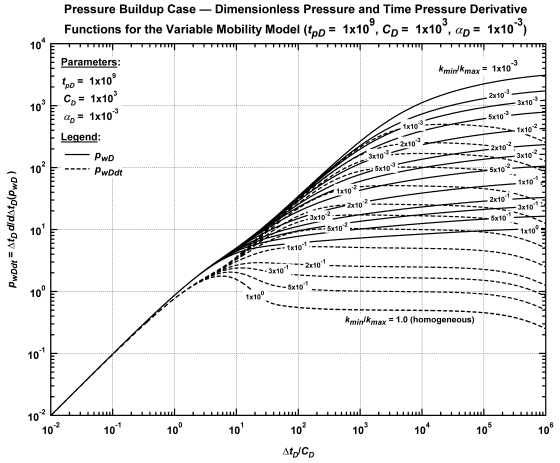

Figure 13c – Type curve plot (p_{wD} and p_{wD}' versus $\Delta t_D/C_D$) — t_{pD} = 1x10^9, C_D = 1x10^3, α_D = 1x10^{-3}, various k_{min}/k_{max} cases.

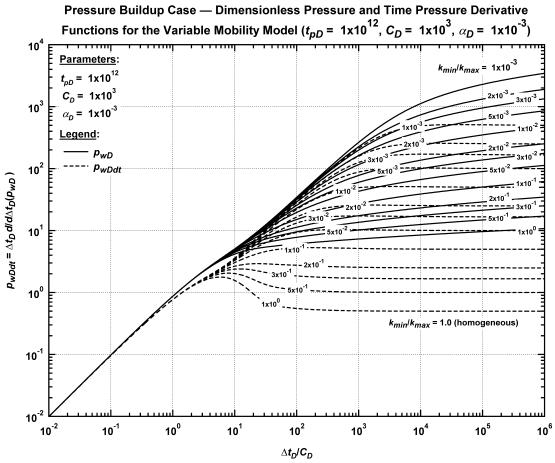

Figure 13d – Type curve plot (p_{wD} and p_{wD}' versus $\Delta t_D/C_D$) — t_{pD} = 1x10^{12}, C_D = 1x10^3, α_D = 1x10^{-3}, various k_{min}/k_{max} cases.

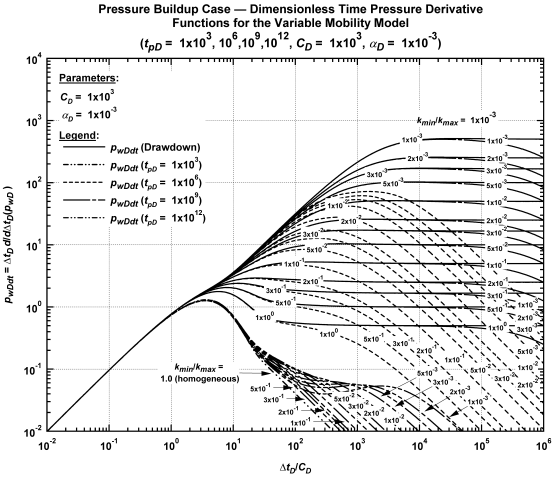

Figure 14 – Buildup type curve plot (p_{wD}' versus $\Delta t_D/C_D$) — t_{pD} = 1x10^3, 10^6, 10^9, 10^{12}, C_D = 1x10^3, α_D = 1x10^{-3}, various k_{min}/k_{max} cases. Note the strong influence of the t_{pD}-parameter (analogous to the homogeneous reservoir case).